Generalized grating equation for virtually-imaged phased-array spectral dispersers

Albert Vega, Andrew M. Weiner, and Christopher Lin

The virtually-imaged phased array (VIPA) is a side-entrance etalon with potential application as a high-resolution spectral disperser for wavelength division multiplexing. Here we present an approximate analytical spectral dispersion law for the VIPA, which we confirm experimentally. © 2003 Optical Society of America

OCIS codes: 230.0230, 050.2230.

Spectral dispersers for spatially separating optical frequencies are important for many applications, including spectroscopy, wavelength division multiplexing (WDM) lightwave communications, and femtosecond pulse shaping. In addition to the well-known prism and diffraction grating, other spectral dispersers that have been developed for wavelength division multiplexing applications include the arrayed waveguide grating[1] and a modified Fabry–Perot etalon named a virtually imaged phased array (VIPA).[2–5] Both the arrayed waveguide grating and the VIPA can provide greater amounts of spectral dispersion than a bulk grating, and the VIPA intrinsically provides very low sensitivity to polarization. Here we discuss the VIPA, which has been much less studied compared to arrayed waveguide gratings. The VIPA is a multiple-beam interference device, and as such is related to the Lummer–Gehrcke plate[6,7] and other multiple-beam interference devices studied in classical optics.[8,9] In recent years several experiments demonstrating the application of VIPAs for wavelength multiplexing-demultiplexing[2] and for dispersion compensation[3,5] have been reported, including system experiments.[10] VIPAs can potentially be used to extend femtosecond pulse shaping[11] to a longer time scale suitable for 40–100 Gb/s lightwave systems. From a theoretical perspective, however, VIPAs have been studied mainly through simulation, and no suitable analytical spectral dispersion relation for the VIPA has been reported. Here, for the first time to our knowledge, we present a generalized grating equation, which constitutes an approximate analytical dispersion law for the VIPA and provide experimental data that confirm our result.

The VIPA, sketched in Fig. 1, operates based on multiple reflections of an input diverging source. Standard etalons used for basic interferometry have two highly reflective coatings that create either an air-spaced or solid cavity.[12] The reflectivities of both coatings are often >95% creating a series of sharp transmission peaks as a function of frequency. For the VIPA, the first or entry-side coating is as close to 100% as possible, but does not cover the entire aperture of the device. The second coating is typically >95%. The input beam is introduced into the VIPA at an angle through the uncoated (or anti reflection) portion of the entry side. The beam is reflected off the second coating back to the coated portion of the entry side. The beam can bounce back and forth between the two coatings resulting in multiple reflections of the input beam. The name virtually imaged phased array comes from the device operating as if there were multiple virtual sources interfering with each other as in a phased array. With any phased array,[13] the direction of the output beam depends on the phase difference between the array elements (virtual sources). Because this phase difference is frequency dependent, the direction of the output beam also varies with frequency; i.e., the VIPA functions as a spectral disperser.

We obtain the spectral dispersion law for the VIPA by comparing the relative phases for the different

A. Vega (e-mail vegaa@purdue.edu) and A. M. Weiner are with the Department of Electrical and Computer Engineering, Purdue University, 465 Northwestern Avenue, Electrical Engineering Building, West Lafayette Indiana 47907-2035. C. Lin is with Avanex Corporation, 40919 Encyclopedia Circle, Fremont, California 94538.

Received 20 November 2002; revised manuscript received 27 March 2003.

0003-6935/03/204152-04$15.00/0

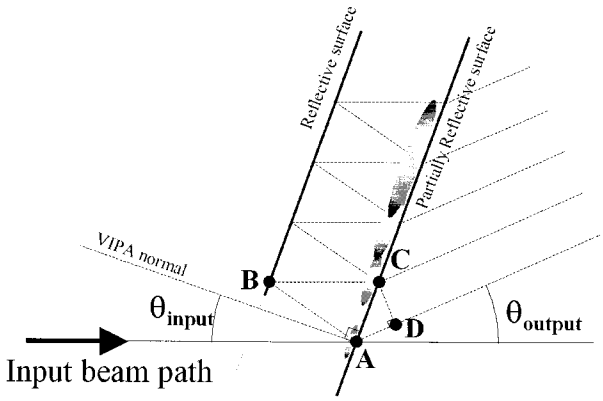

Fig. 1. Schematic diagram of an air-spaced VIPA.

paths shown in Fig. 1. For constructive interference at the output, phase fronts of two parallel paths must match or be a multiple of 2π radians in phase difference. This condition determines the angles at which different wavelengths are emitted from the VIPA. Looking at Fig. 1, we determine that the constructive interference condition is met when the phase change from paths $\overline{ABC}$ and $\overline{AD}$ differs by a multiple of 2π. From this difference we obtain, for an air-spaced etalon, the following expression:

$$\omega \frac{2L}{c}\left[\frac{1}{\cos\theta_{\text{input}}} - \tan\theta_{\text{input}}\sin(\theta_{\text{input}} + \theta_{\text{output}})\right] = 2m\pi, \quad (1)$$

where L is the thickness of the VIPA, c is the speed of light, ω is the frequency in radians, m is an integer and gives the order number, and θ_{input} and θ_{output} are the input angle and output (observation) angle, respectively, of the VIPA, also shown in Fig. 1. Note that according to our definition, $\theta_{\text{output}} = 0$ corresponds to an observation along the same direction as the input beam. Equation (1) is applicable to large as well as small angles. This expression, which gives the output (diffracted) angle in terms of the input angle and the diffraction order, may be regarded as a generalized grating equation applicable to the VIPA.

Although several experimental and simulation-based studies of VIPAs have been published,[2–5,10] an equation similar to Eq. (1) has not been previously reported. In one publication,[5] the spectral dispersion relation was written in a form equivalent to $\omega(2L/c)\cos\theta_{\text{output}} = 2m\pi$ (this is for the case of an air-spaced etalon, $n = 1$). This is simply the transmission resonance condition for a standard Fabry–Perot. However, we note that unlike Eq. (1), the result from Ref. 5 is a function of one angular variable only and is therefore inadequate to describe the full spectral dispersion behavior of the VIPA, which is a function of both input and output angles.

Returning now to Eq. (1), we can obtain a formula for the free spectral range (FSR) of the VIPA. By looking at adjacent orders we obtain the following relation:

$$FSR = \frac{c}{2L}\left[\frac{1}{\cos\theta_{\text{input}}} - \tan\theta_{\text{input}}\sin(\theta_{\text{input}} + \theta_{\text{output}})\right]^{-1}. \quad (2)$$

This is significantly different than the expression for the FSR of a standard etalon.[14] The free spectral range can easily be obtained from experimental measurements (described below). Therefore we will use FSR data for a quantitative test of our spectral dispersion law.

We have also obtained an analogous relation for solid etalons, where we are also concerned with the internal angle inside the cavity of the VIPA. The relation of the internal angle and input angle is given by Snell's Law [$\sin(\theta_{\text{input}}) = n^* \sin(\theta_{\text{internal}})$] at the air-cavity interfaces. The result when incorporated into an equation similar to Eq. (1) is

$$\omega \frac{2L}{c}\left[\frac{n}{\cos\theta_{\text{internal}}} - \tan\theta_{\text{internal}}\sin(\theta_{\text{input}} + \theta_{\text{output}})\right] = 2m\pi, \quad (3)$$

where n is the index of refraction of the solid etalon material.

It is worth mentioning several assumptions made in deriving our spectral dispersion law. First, the Gouy phase shift (the π phase shift acquired during propagation through the focus of a Gaussian beam) is ignored. Second, we neglect the change in the spot size from one reflection to the next (all the virtual sources are taken as identical). These assumptions are reasonable for typical operating regimes with a large number of virtual sources. Third, we ignore any frequency-dependent phase shifts associated with reflections inside the VIPA. In general, reflections from a dielectric multilayer mirror give rise to phase shifts that depend on input angle, polarization (except for normal incidence), and frequency. However, as long as the dielectric mirrors are utilized near the center of their high-reflectivity band, such phase shifts (and especially the frequency dispersion of such phase shift) are expected to be small.[15] This justifies our neglect of such effects. Furthermore, these assumptions are validated by data (shown below), which are in excellent agreement with our proposed spectral dispersion law.

Measurements are performed with either a tunable external cavity diode laser or an erbium fiber-based amplified spontaneous emission source providing ~40 nm of bandwidth. A fiber collimator was used to collimate the source, which was focused to a line by a cylindrical lens and directed into the VIPA through the noncoated or antireflection-coated region of the entry side. The etalon was placed on a fine rotation stage to control the input angle. A 190-cm focal length achromatic lens was placed one focal length behind the output side of the etalon to convert the

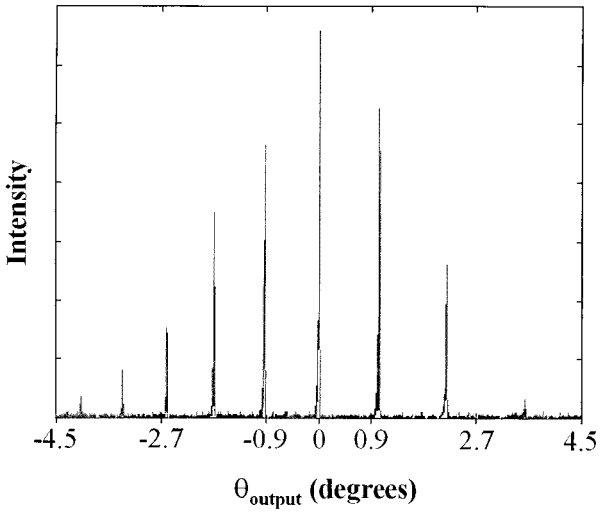

Fig. 2. Spatial intensity profile for a 0.375-mm thick air-spaced VIPA, measured at the back focal plane of Fourier-transform lens, with $\theta_{input} = 8.6°$ and input wavelength of 1546.5 nm.

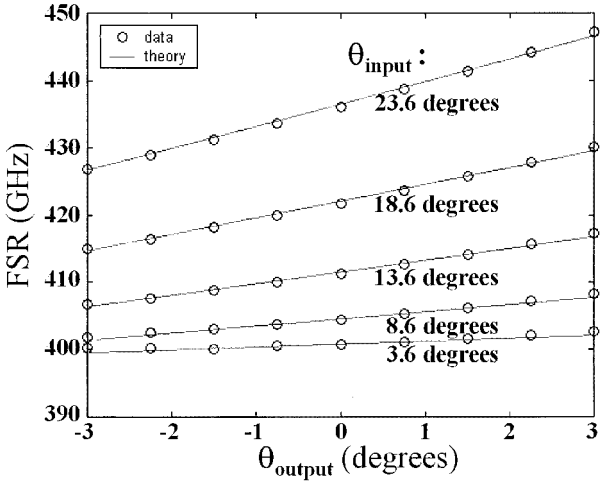

Fig. 4. Measured (symbols) and calculated (solid lines) FSR for air-spaced VIPA, for various input and output angles. VIPA air-gap thickness is 375 μm.

output angular distribution of the VIPA into a spatial distribution. A single-mode fiber placed on a computer controlled translation stage was positioned one focal length behind this Fourier-transform lens to sample the output light. The single-mode fiber could be connected to a power meter to record the output spatial distribution for a fixed wavelength source or to an optical spectrum analyzer (0.01 nm spectral resolution) to record the output power spectrum as a function of position for the amplified spontaneous emission source.

Figures 2 and 3 show examples of our data for a 0.375-mm thick air-spaced VIPA (Avanex). The front surface of the etalon had an estimated reflectivity of >99.9% over much of the front surface, an AR-coated entry region on the remainder of the front surface, an estimated 98.4% back surface reflectivity, and an ≈13 mm clear aperture. Figure 2 shows the spatial profile of the output intensity for a fixed input wavelength of 1546.50 nm and $\theta_{input} = 8.6°$. Several diffraction orders are visible over a range of roughly ±3 degrees. For Fig. 3, we used the ASE source and an optical spectrum analyzer to measure the output spectrum of the VIPA, with $\theta_{input} = 11.1°$, at several different closely spaced spatial positions near the central order (i.e., near the $\theta_{output} = 0$ point). At each spatial position, the spectrum is periodically peaked with a FSR on the order of 400 GHz (3.2 nm), similar to the behavior of a standard Fabry–Perot. However, unlike a standard Fabry–Perot that acts as a narrow-band transmission filter, the VIPA clearly functions as a spectral disperser. The peaks translate in optical frequency as the output observation angle is tuned.

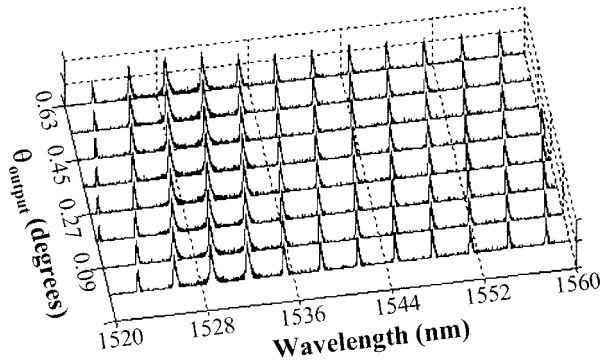

Fig. 3. Output power spectra for air-spaced VIPA, measured with broadband input and $\theta_{input} = 11.1°$, for various output angles (i.e., various spatial positions of the output sampling fiber).

Our spectral dispersion law is able to predict the behavior of the VIPA not only for the central order ($\theta_{output} \approx 0$), but also for the other diffraction orders and for various input angles. Figure 4 shows FSR data for the air-spaced VIPA, extracted from data such as those in Fig. 3, for various input angles and output observation angles. The experimental data are plotted as open circles overlaying the theoretical curves from Eq. (2). The repeatability of our FSR measurements, determined by taking multiple sets of data for a certain fixed input angle, is extremely good, with an estimated error of less than 100 MHz. Before comparing the data with the theory, we first performed independent measurements to determine the $\theta_{input} = 0$ and $\theta_{output} = 0$ positions. We estimate an accuracy of ±0.4° and less than ±0.2° in our absolute determination of θ_{input} and θ_{output}, respectively. Relative values of θ_{input} and θ_{output} could then be controlled precisely by use of the rotation stage for θ_{input} and the computer-controlled translation stage for θ_{output}. In fitting the data, we introduced a single fine shift of the $\theta_{input} = 0$ position and a single fine shift of the $\theta_{output} = 0$ position to obtain the best global overlap between all the data and theoretical curves. We also took the FSR, extrapolated to the case of $\theta_{input} = 0$, as a fit parameter, to account for any small uncertainty in etalon thickness. The

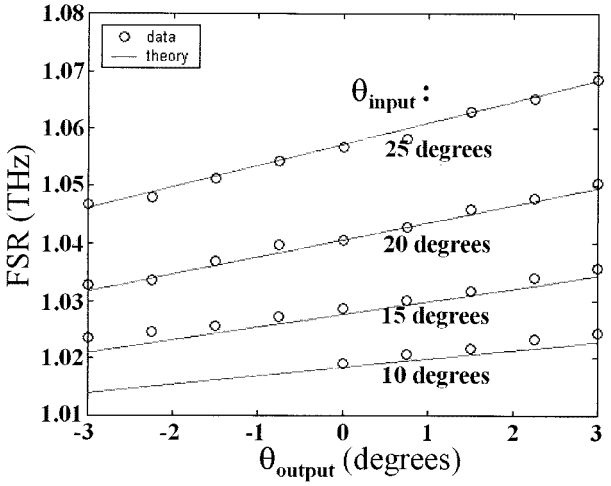

Fig. 5. Measured (symbols) and calculated (solid lines) FSR for solid VIPA, for various input and output angles. VIPA thickness is 100 μm.

agreement between the data and theory is extremely good. The theory fully and quantitatively predicts the variation in FSR as a function of both input and output angles over the full range of parameters we investigated.

We have performed similar experiments with a 0.1-mm thick solid etalon (TecOptics), constructed of Suprasil 2 fused silica and with a 20-mm aperture. The entry side of the etalon was covered with a coating with a reflectivity of >99.5% for wavelengths 1520–1580 nm. This coating only covered 75% of the aperture leaving an uncoated window for coupling in the input beam. On the output side of the VIPA, a coating with reflectivity of 97% ± 1% for wavelengths 1520–1580 nm covered the entire aperture of the device. Figure 5 shows the FSR data for the solid VIPA. The theoretical curves were computed based on Eq. (3), approximating the refractive index n as a constant. Theoretical curves computed by use of a Sellmeier equation for the wavelength-dependent refractive index showed no visual change for the experimental wavelength range when compared with those in Fig. 5. The theory is once again in excellent agreement with the measurements. These results provide a strong experimental confirmation of the proposed spectral dispersion law for different VIPA constructions.

In summary, we have proposed and experimentally confirmed an approximate analytic spectral dispersion law for virtual-imaged phased-array (VIPA) spectral dispersers. Our formulation includes the dependence on both input and observation angles and on diffraction order. Our results should contribute to the further application of these devices both for lightwave communications as well as for other applications such as ultrafast optical pulse shaping.

This material is based upon work supported in part by the U.S. Army Research Office under contract DAAD19-00-0497 and the National Science Foundation under contract 0100949-ECS. We gratefully acknowledge D. E. Leaird for assistance.

References

1. K. Okamoto, Opt. and Quant. Elec. **31,** 107–129 (1999).
2. M. Shirasaki, Opt. Lett. **21,** 366–368 (1996).
3. M. Shirasaki, IEEE Phot. Tech. Lett. **9,** 1598–1560 (1997).
4. M. Shirasaki, A. N. Akhter, and C. Lin, IEEE Phot. Tech. Lett. **11,** 1443–1445 (1999).
5. M. Shirasaki and S. Cao, OSA Trends in Optics and Photonics (TOPS) Vol 54, Optical Fiber Communication Conference, Technical Digest, Postconference Edition (Optical Society of America, Washington DC 2001), TuSI pp 1–3.
6. O. Lummer and E. Gehrcke, Ann. D. Physik, **10,** 457–477 (1903).
7. M. Born and E. Wolf, *Principles of Optics* (Cambridge University, Cambridge, UK, 1999), pp. 380–386.
8. C. Dufour, Rev. d'Opt **24,** 11–18 (1945).
9. Y. T. Mazurenko, Opt. Spectr. **69,** 241–243 (1990).
10. M. Shirasaki, Y. Kawahata, S. Cao, H. Ooi, N. Mitamura, H. Isono, G. Ishikawa, G. Barbarossa, C. Yang, and C. Lin, *European Conference on Optical Communications* (ECOC2000), Postdeadline paper 2.3.
11. A. M. Weiner, Rev. Sci. Instr. **71,** 1929–1960 (2000).
12. E. Hecht, *Optics* (Addison Wesley, Reading, Mass. 1998), pp. 413–416.
13. S. Ramo, J. R. Whinnery, and T. Van Duzer, *Fields and Waves in Communication Electronics* (Wiley, New York, 1993), pp. 630–637.
14. J. M. Vaughan, *The Fabry–Perot Interferometer* (Adam Hilger, Bristol, 1989), pp. 104–105.
15. S. DeSilvestri, P. Laporta, and A. Svelto, Opt. Lett. **9,** 335–337 (1984).